Published paper

S. Stipetic, D. Zarko and M. Kovacic, "Optimised design of permanent magnet assisted synchronous reluctance motor series using combined analytical–finite element analysis based approach," in *IET Electric Power Applications*, vol. 10, no. 5, pp. 330-338, 5 2016.
http://dx.doi.org/10.1049/iet-epa.2015.0245

Optimised design of permanent magnet assisted synchronous reluctance motor series using combined analytical–finite element analysis based approach

Stjepan Stipetic, Damir Zarko, Marinko Kovacic

stjepan.stipetic@fer.hr,
damir.zarko@fer.hr,
marinko.kovacic@fer.hr
University of Zagreb
Faculty of Electrical Engineering and Computing,
Department of Electrical Machines, Drives and Automation
Address: Unska 3, 10000 Zagreb, Croatia

This paper presents a comprehensive approach to design of series of permanent magnet assisted synchronous reluctance motors using combined analytical and finite element calculations. A global optimization metaheuristic algorithm (Differential Evolution) is utilized in order to achieve optimal design in terms of maximum torque per volume with numerous specific boundaries imposed on motor geometry and performance. A novel approach to calculation of the specified constant power speed range and demagnetization effect in sudden symmetrical short circuit using iterative finite element magnetostatic simulations is presented. Based on the results of optimized design, a 100 kW prototype was built and tested.

Introduction: Permanent magnet (assisted) synchronous reluctance (PMSynRM, PMSynRel, PMASR, PMSR) machines attract more attention due to high efficiency and wide constant power speed range which make this motor type an alternative to both interior permanent magnet (IPM) motors and induction motors in terms of cost and performance [1, 2]. A weak definition considers that PMSynRM motor is an IPM motor characterized by high magnetic anisotropy and a reduced PM volume while a stronger definition considers that the higher torque component of the motor is the reluctance torque [3, 4]. As stated in [5], this motor is ideal for traction applications such as electrical vehicles.

Various authors conducted recent studies on topics related to PMSynRM machines: rotor design [6–8], usage of ferrite [9] or NdFeB magnets [10], flux weakening performance [11], rotor bridge design [12], acoustic behaviour [13] etc.

This research was motivated by the requirement to design a series of PMSynRM motors of power ratings 50 kW, 75 kW and 100 kW at 3000 rpm and 400 V which will fit into the housing (IEC180 frame size) of an existing 2 pole 30 kW induction motor. All the machines should have constant power range up to 4500 rpm (CPSR - constant power speed ratio of 1.5) and the highest rated machine should comply with the IE4 efficiency requirement (95.6 %). All the machines in the series will have the same lamination design but different stack length and number of turns connected in series depending on the torque rating or the rated speed.

A mathematical optimization procedure utilizing combined analytical-finite element (FE) electromagnetic calculation is used to obtain so called *reference design*, described in detail in [14]. Analytical axial scaling laws ([14, 15]) are then used to recalculate the parameters of the reference design for all the required power ratings. The objective (goal, cost) function of the optimization algorithm is maximization of torque per volume. Although thermal and mechanical calculations can be introduced inside an optimization loop to fully utilize the multiphysics approach, they were conducted in post-optimization stage, i.e. as single shot calculations performed on the optimized design. A 100 kW prototype was built based on the results of optimization procedure and tested.

Optimization setup: Finding an electrical machine design that will satisfy all the requirements and constraints can be an overwhelming task due to a large number of parameters whose effects on the motor performance and quality of the design are strongly coupled. There is an obvious need for a systematic approach to decision making in the design process based on an iterative scheme that would gradually lead to a solution which satisfies the imposed constraints and minimizes (or maximizes) some objective function (e.g. torque density, active volume, cost, efficiency etc.). This approach is called mathematical optimization, a very important design tool which helps designers to push the existing invisible design boundaries while using available materials and technology.

An optimization problem is set up to find the vector of variables

$$\mathbf{X} = (x_1, \ldots, x_D), \qquad \mathbf{X} \in R^D \tag{1}$$

where every variable is bounded by lower and upper boundary $x^{(L)}$ and $x^{(U)}$, i.e.

$$x_j^{(L)} \leq x_j \leq x_j^{(U)} \qquad j = 1, \ldots, D, \tag{2}$$

which minimizes the objective function

$$f(\mathbf{X}), \tag{3}$$

and satisfies m inequality constraints

$$g_j\,(\mathbf{X}) \leq 0,\ j = 1, \ldots, m. \tag{4}$$

The algorithm that was used in this case is Differential Evolution (DE), first introduced by Price and Storn [16] in 1995, which belongs to the class of evolutionary algorithms and is widely utilized in the field of electrical machines ([14, 17–22]).

In short, the DE method works on a population (generation) which is a set of NP individuals (members), where each individual presents one machine design. Initial population is randomly populated inside the boundary constraints $x^{(L)}$ and $x^{(U)}$ of each vector. The candidate (trial) population is obtained by crossover and mutation processes from the existing population. The next generation is obtained by comparing the existing and candidate population and choosing members that satisfy inequality constraints and yield better value of the objective function.

It is a good practice to choose variables which are given as non-dimensional ratios of related geometrical parameters, for example ratio of slot depth to difference between stator outer radius and stator inner radius etc. This helps in creating geometrically feasible or "drawable" geometries without negative lengths or incorrect intersections of various geometric regions, and allows the extension of results from the studied configuration to a similar one with different number of poles and slots [23].

In this particular case, the vector of machine variables ($\mathbf{X}$) is:

1. D_s/D_{out} - ratio of stator inner diameter to stator outer diameter,
2. $h_{ys}/[(D_{out} - D_s)/2]$ - ratio of yoke thickness to difference between stator outer and inner radius,
3. b_t/τ_u - ratio of tooth width to slot pitch at stator inner diameter,
4. λ_m - ratio of total cavity (space in the radial direction occupied by permanent magnets) to total rotor depth (space between rotor surface and inner diameter of rotor lamination),
5. λ_{md1} - percentage of total rotor depth for the outermost rotor core section (space between rotor surface and the outer layer of cavities),
6. λ_{md2} - percentage of total rotor depth for middle rotor core section (space between inner and outer layer of cavities),
7. β/β_0 - angle of the slanted magnet relative to the maximum allowed angle of the slanted magnet ($\beta_0 = 0.5\pi(1 - 1/p)$),
8. λ_p - angular span of the inner cavity relative to the pole pitch.

Lower and upper boundary constraints of the variables are:

$$\begin{aligned}
0.45 \leq & D_s/D_{out} \leq 0.75,\\
0.2 \leq & h_{ys}/[(D_{out} - D_s)/2] \leq 0.6,\\
0.3 \leq & b_t/\tau_u \leq 0.7,\\
0.05 \leq & \lambda_m \leq 0.5,\\
0.2 \leq & \lambda_{md1} \leq 0.6,\\
0.05 \leq & \lambda_{md2} \leq 0.4,\\
0.5 \leq & \beta/\beta_0 \leq 1.0,\\
0.75 \leq & \lambda_p \leq 0.95.
\end{aligned}$$

Variables with constant value, i.e. design parameters that do not change during the optimization procedure (preset parameters) according to Fig. 1 are:

1. δ = 0.8 mm - air-gap length,

2. D_{out} = 270 mm - stator outer diameter,
3. l_{stk} = 312 mm - stack length,
4. D_{in} = 85 mm - rotor inner diameter (shaft diameter),
5. b_o = 2.5 mm - slot opening width,
6. d_o = 1 mm - slot opening height,
7. r_c = 1.2 mm - slot bottom radius,
8. N_s = 33 - number of stator slots,
9. p = 4 - number of pole pairs,
10. k_{Cu} = 0.4 - slot fill factor,
11. J = 6 A/mm^2 - slot current density,
12. N_{m1} = 2 - number of magnet plates in outer layer,
13. N_{m2} = 3 - number of magnet plates in inner layer,
14. d_b = 4 mm - rotor bolt diameter,
15. a_p = 1 - number of parallel paths,
16. n_c= 1 - number of turns per coil,
17. n_n = 3000 min^{-1} - rated speed,
18. n_{max} = 4500 min^{-1} - maximum speed in constant power range,
19. d_{r0} = 1 mm - rotor bridge thickness (at the rotor surface),
20. d_{r1} = 1 mm - rotor bridge thickness (between magnets in the outer layer),
21. d_{r2} = 0.8 mm - rotor bridge thickness (between magnets in the inner layer).

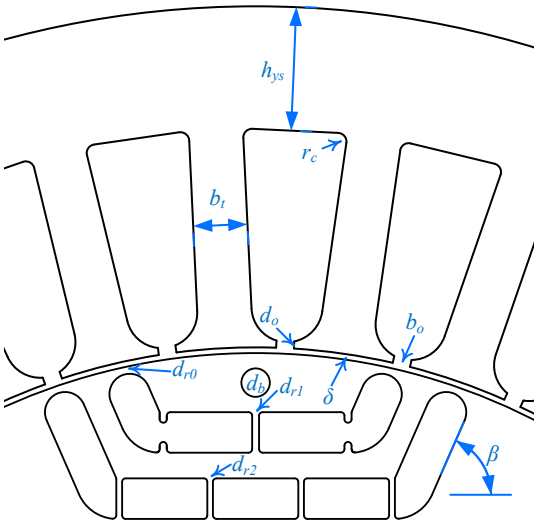

Fig. 1: Lamination cross section of a reference design

As advised in [24], constraint functions may be of widely differing magnitudes. Such differences may make some boundary functions more sensitive than others in the optimization process, possibly leading to failures to converge. For this reason, it is advisable to normalize all functions by choosing suitable base values and expressing all quantities in per unit of those base values.

A good base value is in fact the minimum or maximum value of the imposed constraint. For example, for the minimum efficiency boundary the constraint function would be

$$\eta_{con}(\mathbf{X}) = 1 - \frac{\eta(\mathbf{X})}{\eta_{min}}, \tag{5}$$

and for the maximum tooth flux density

$$B_{st,con}(\mathbf{X}) = \frac{B_{st}(\mathbf{X})}{B_{st,max}} - 1 \tag{6}$$

where $\eta(\mathbf{X})$ and $B_{st}(\mathbf{X})$ are the efficiency and the tooth flux density of the motor design defined by vector $\mathbf{X}$, η_{min} is the minimum allowed efficiency and $B_{st,max}$ is the maximum allowed tooth flux density.

Inequality constraint functions in this particular case are:

- $B_{st} \leq$ 1.8 T - maximum allowed average stator tooth flux density
- $B_{sy} \leq$ 1.3 T - maximum allowed stator yoke flux density
- $\eta \geq$ 95.6 % - minimum required efficiency (IE4)
- $A \leq$ 55000 A/m - maximum allowed linear current density along stator bore
- $P_{tot} \leq$ 4590 W - maximum allowed total loss (limited by heat transfer capability of the fan cooled housing),
- $P_{out\omega_{max}} \geq P_{out\omega_r}$ - power output at maximum speed in constant power speed range must be at least equal to rated power,
- $\cos\varphi \geq$ 0.8 - minimum required power factor at rated load
- $B_m \geq$ 0.2 T - minimum allowed magnet flux density during sudden short circuit at rated speed and load

Widely accepted technique to efficiently handle boundary functions in DE is Lampinen's criterion [25]. The main advantages of this approach are: it forces the selection towards feasible regions where constraints are satisfied thus resulting in faster convergence, it saves time since no evaluation of the objective function occurs if constraints are violated.

Furthermore, if any of the boundary constraints is violated, other boundary constraints are not even calculated at all, which is especially interesting for computationally expensive calculations. In this particular case the boundary constraints are listed from computationally least expensive (g_1) to computationally most expensive (g_4), which is also the sequence in which they are evaluated during optimization process.

- g_1 - analytical calculation of linear current density
- g_2 - rated load
- g_3 - CPSR (power at maximum speed)
- g_4 - demagnetization

Quite often a number of turns per coil is selected as an optimization parameter when dealing with synchronous PM or reluctance machines. This is essentially a bad approach for optimization procedures that use current driven FE simulations (both magnetostatic and transient). Since magnetic field solution and torque production depend on the current density imposed through conductive regions and on their area, it is enough to use the winding with one turn per coil and one parallel path as described in [14, 26]. In that case current density can be set to a constant value or it can be varied as an optimization variable. When the performance parameters are to be extracted (e.g. inductance, behaviour in flux weakening region, back EMF), it is easy to find the appropriate number of turns per coil and parallel paths to match the inverter or grid voltage capability [15].

However, if the optimization procedure involves multiphysics simulations with coupled electromagnetic-thermal calculations, the number of turns per coil may be important in some cases like the drive cycle simulations of a traction motor as described in [27]. In addition, the number of conductors (in form wound stator coils) or conductor strands (in random wound stator coils) in the slot may be required for accurate representation of the winding by the layered or cuboid thermal model.

The consideration of IPM current control angle γ (angle between current vector and q axis with permanent magnet flux vector aligned with the d axis) is addressed differently throughout the literature. One approach is to make a simulation for several current angles γ, do a polynomial fit, find an optimum angle to achieve the maximum torque per amp (MTPA) operation, then resolve the model using this optimal angle [14]. This is particularly significant if additional simulations with optimal angle γ are to be performed (e.g. demagnetization check, calculation of iron losses, tooth or yoke flux density etc.). This angle for MTPA operation can be calculated from minimum number of calculations using approximate relations [28] or can be included as an optimization parameter [29]. Sometimes current vector is kept the same as in the reference solution [30], which saves time, but affects the accuracy.

Optimization procedure and novelties: The order of operations inside optimization procedure required for calculation of one specific design (population member of one generation of vectors) using finite element method, is as follows:

1. calculation of geometric parameters from the vector of machine variables and geometrical feasibility check

2. FE pre-processing stage which includes parametrized creation of motor geometry, definition of motor regions depending on assigned material (air, iron, magnet, coil), setting of current densities in the coil regions and directions of magnetization for permanent magnets, generating FE mesh
3. analytical calculation of linear current density
4. iterative magnetostatic FE calculation of flux linkages, electromagnetic torque, inductances and iron losses at rated speed and angle γ determined to satisfy *MTPA - max torque per amp* for a given slot current density
5. analytical calulation of end winding inductance
6. analytical calculation of winding resistance and terminal voltage
7. iterative magnetostatic FE calculation of flux linkages, electromagnetic torque, current vector (defined by angle $\gamma_{\omega_{max}}$ and magnitude) and shaft power at maximum speed of CPSR with maximum utilization of the available DC link voltage
8. iterative magnetostatic FE calculation of demagnetization of PMs at sudden three-phase short circuit at motor terminals
9. approximate magnetostatic FE calculation of back EMF THD
10. analytical calculation of copper losses, mechanical losses and efficiency

Finite element magnetostatic calculation of demagnetization effect

One particular requirement for this motor design is the capability to withstand a symmetrical short circuit (SSC) at its terminals in the motoring operation mode without irreversible demagnetization of its permanent magnets. The level of demagnetization will depend on the peak transient value of the short-circuit current producing armature winding flux in the direction of negative d axis, thus opposing the permanent magnet flux and causing potentially hazardous demagnetization below the knee point of the magnet's temperature dependent BH curve. The peak transient SSC current depends on the operating point of the motor at the time instant when the short circuit is triggered. The detailed analysis presented in [31] indicates that the worst operating point resulting in the highest peak current is the point at rated speed and torque in regenerative operation mode. The term rated speed refers to the speed at which the maximum available voltage from the inverter has been reached. Beyond that speed the flux weakening must be utilized to maintain constant voltage at motor terminals while constant torque can no longer be maintained.

The transient FE simulation with rotor motion is time consuming so it cannot be used during optimization to calculate the peak transient SSC current. Instead, an iterative scheme is used in this case relying only on magnetostatic simulations with fixed rotor position. This scheme consists of the following steps:

1 Create and solve a magnetostatic FE model of the motor (one candidate vector in the optimization scheme) at rated speed with current vector set to an optimal position for MTPA operation. The magnitude of the current vector is defined by current density (set to a constant value in our case) multiplied with slot area and slot fill factor.

2 Calculate complex stator flux vector $\mathbf{\Psi_s} = \Psi_s e^{\mathrm{j}\alpha_s}$ from the FE model. A detailed description of the procedure for calculating $\mathbf{\Psi_s}$ from 2D FE model is available in [32].

3 Freeze permeabilities in the nodes of the FE mesh and calculate inductances L_d, L_q and complex permanent magnet flux vector $\mathbf{\Psi_m} = \Psi_m e^{\mathrm{j}\alpha_m}$ using the method from [32].

4 Calculate initial peak value of the transient SSC current using [31]

$$I_{scmax} = \frac{|\mathbf{\Psi_m}|}{L_d} + e^{-\frac{t_{max}}{\tau}} \frac{|\mathbf{\Psi_s}|}{L_d} \quad (7)$$

$$t_{max} = \frac{\pi + \alpha_s - \alpha_m}{\omega} \quad (8)$$

$$\tau = \frac{2L_dL_q}{R_s\,(L_d + L_q)} \quad (9)$$

where R_S is the stator winding resistance, τ is the decaying time constant of transient stator current magnitude, and t_{max} is the time needed for the rotating PM flux vector (assuming that rotor retains its synchronous speed) to reach the position where it points in the opposite direction from the direction of stator flux vector at the time instant ($t = 0$) when SSC occurred. In this position the maximum stator current will flow to compensate the difference between stator and PM flux vectors as indicated in Fig. 2. An approximation is used in these equations which assumes that the angle of the stator flux vector in stator-fixed coordinate system ($\alpha\beta$) remains unchanged while its magnitude is decaying with the time constant τ [31].

Thus calculated initial peak transient SSC current is not correct since it was obtained using L_d, L_q, $\mathbf{\Psi_s}$ and $\mathbf{\Psi_m}$ extracted from the rated operating point prior to short circuit. Therefore, the saturation level in the motor did not correspond to the actual saturation level when maximum SSC current is flowing.

5 New FE simulation is carried out using initially calculated I_{scmax} as the phase current magnitude with instantaneous phase currents in slots set to values that will result in the stator current vector pointing in the negative d axis direction (opposing the permanent magnet field) as shown in Fig. 2. By freezing the permeabilities from this simulation the steps 2, 3 and 4 are repeated and new value of I_{scmax} is calculated. The new peak transient SSC current is compared to its predecessor and if their difference is smaller than some initially prescribed margin, e.g. 0.5 %, the last calculated I_{scmax} is the result. If the difference is greater than the margin, step 5 is repeated always using I_{scmax} from the previous iteration until the difference between peak transient SSC currents from two consecutive iterations is smaller than the margin.

In our case it took only six magnetostatic simulations in step 5 to calculate I_{scmax} within the margin of 0.5 %. The peak transient SSC current calculated using this procedure for the optimized motor geometry in Fig. 7a equals 1109 A. For comparison, a transient 2D FE simulation of SSC with rotor motion carried out using Infolytica MagNet software produces the transient current response shown in Fig. 3 with peak current equal to 1138 A, which is a 2.5% difference from the current obtained from iterative magnetostatic simulations.

6 From the last FE simulation in step 5 with current vector magnitude I_{scmax} pointing in the direction of negative d axis calculate minimum flux density across every magnet and compare to a predefined constraint. This constraint represents the minimum allowed flux density in the magnet B_{PMmin} at the steady state working temperature of magnets. The value of B_{PMmin} should be set to a flux density in the 2^{nd} quadrant of the magnet's BH demagnetization curve where the straight portion of the curve ends before the knee of the curve start forming ($B_{PMdemag}$) increased by a safety margin (in our case 0.2 T).

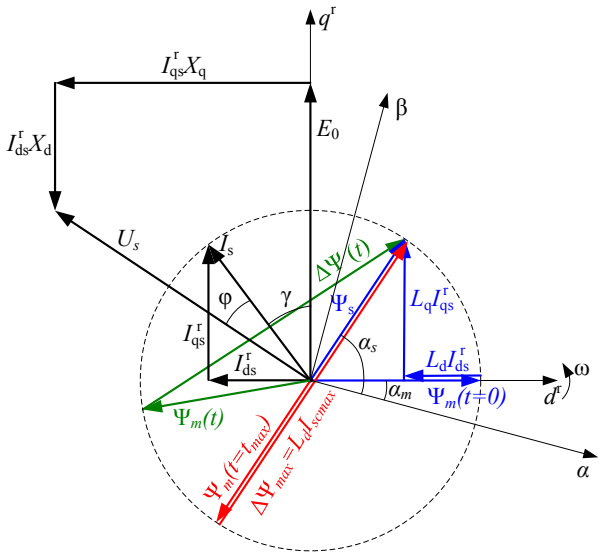

Fig. 2: Phasor diagram at rated load and flux vectors at various time instants during SSC

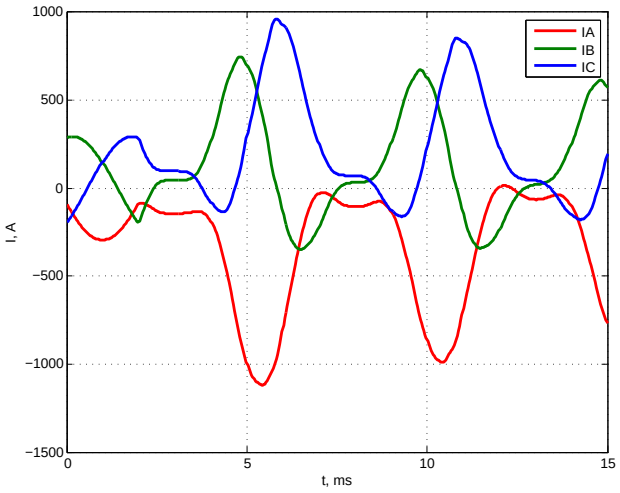

Fig. 3: Waveform of sudden three-phase short-circuit current calculated using transient 2D FE simulation with rotor motion

Magnetostatic calculation of power at maximum speed

The PMSynRMs are typically designed for wide speed operation in constant power mode. The speed range within which it will be possible to maintain constant power is dependent on motor geometry, i.e. primarily on per-unit permanent magnet flux and saliency ratio. Therefore, the CPSR is set as a design requirement that needs to be fulfilled and as such is included in the list of inequality constraints of the optimization problem. The CPSR is checked by calculating the maximum shaft power that a particular population member (motor design) develops at maximum required speed utilizing maximum available voltage from the inverter while magnitude of the current vector is limited by rated current of the motor. A good indicator of flux weakening capability of a PMSynRM is per-unit value of its characteristic current defined as $I_c = \Psi_m/(L_d I_{mr})$, where Ψ_m is the magnitude of permanent magnet flux vector, L_d is the d axis inductance and I_{mr} is the magnitude of rated stator current vector. According to the theory presented in [33] and [34], a PMSynRM can have either finite or infinite theoretical maximum speed limit. In the case of finite speed limit (motors with $I_c > 1$), the drive is operated with rated current at the minimum current angle required to give rated terminal voltage, i.e. at the intersection of the voltage and current-limit loci. In that case it is sufficient to keep the current at rated value and find the position of the current vector (angle γ) at which rated terminal voltage is reached. In the case of infinite speed limit (motors with $I_c \leq 1$), the drive operates to give maximum torque with a limited voltage, which is also known as Maximum Torque per Voltage (MTPV) control strategy. In that case the current vector angle $\gamma_{\omega_{max}}$ and the its magnitude $I_{m\omega_{max}}$ must be varied to calculate the point where the constant torque hyperbola is tangent to the voltage-limit ellipse. The algorithm described hereafter is suitable for finding the operating point at maximum speed for either finite or infinite speed motors because it varies simultaneously the control angle and the magnitude of the current vector and finds their values at which maximum available voltage from the inverter is fully utilized and maximum available torque is produced by the motor.

Finding the position $\gamma_{\omega_{max}}$ and magnitude $I_{m\omega_{max}}$ of the current vector for which the voltage limit is reached and maximum attainable power and torque output are obtained at maximum required speed is not a problem that can be solved in a single FE simulation. An iterative approach is required which can be done in the following steps assuming that Matlab 2 is used as a programming environment:

1 In an initial step the values for d and q axis components of PM flux linkage (Ψ_{md}, Ψ_{mq}), stator inductances (L_d, L_q), including cross saturation component (L_{dq}), should be extracted by freezing the permeabilities from FE magnetostatic simulation at rated speed [32]. Using a constrained nonlinear optimization (Matlab function *fmincon*) subjected to the nonlinear equality constraint $ceq(x) = 0$ (voltage at maximum speed equal to voltage at rated speed) to solve an optimization problem with cost function equal to

$$F_c = \frac{P_{em\omega_r} - P_{em\omega_{max}}}{P_{em\omega_r}} \tag{10}$$

where $P_{em\omega_r}$ is the electromagnetic power output at rated speed and $P_{em\omega_{max}}$ is the electromagnetic power output at maximum speed. The minimization of this cost function actually maximizes $P_{em\omega_{max}}$ which is our goal. The term electromagnetic power refers to the power output without subtracting the power loss components due to core losses and mechanical losses. This subtraction is normally done if one wants to calculate the actual shaft power. The electromagnetic power is used to avoid calculation of core losses within constrained nonlinear optimization (CNO), since core loss calculation requires running FE simulations. In this manner the CNO is performed very quickly since it uses constant motor parameters extracted using permeability freezing.

The power output $P_{em\omega_{max}}$ is calculated within Matlab function called by *fmnicon* command using the following equations:

$$I_{dm\omega_{max}} = I_{m\omega_{max}} \sin(\gamma_{\omega_{max}}) \tag{11}$$

$$I_{qm\omega_{max}} = I_{m\omega_{max}} \cos(\gamma_{\omega_{max}}) \tag{12}$$

$$\Psi_{d\omega_{max}} = \Psi_{md} + L_d I_{dm\omega_{max}} + L_{dq} I_{qm\omega_{max}} \tag{13}$$

$$\Psi_{q\omega_{max}} = \Psi_{mq} + L_q I_{qm\omega_{max}} + L_{dq} I_{dm\omega_{max}} \tag{14}$$

$$T_{em\omega_{max}} = \frac{3}{2} p \left(\Psi_{d\omega_{max}} I_{qm\omega_{max}} - \Psi_{q\omega_{max}} I_{dm\omega_{max}}\right) \tag{15}$$

$$P_{em\omega_{max}} = T_{em\omega_{max}} \frac{\omega_{max}}{p} \tag{16}$$

where $T_{em\omega max}$ is the electromagnetic torque at maximum speed, p is the number of pole pairs, and ω_{max} is the maximum electrical synchronous speed. The values of $I_{m\omega_{max}}$ and $\gamma_{\omega_{max}}$ are varied inside the optimization algorithm to minimize F_c. The electromagnetic power output at rated speed $P_{em\omega_r}$ is used as an input parameter and is calculated outside CNO using the same equations, but with rated current magnitude I_{mr} and rated current control angle γ_r. The angle γ_r is calculated using the polynomial approach described in the previous section.

In addition, the nonlinear equality constraint $ceq(x) = 0$ must be satisfied which is defined in a separate Matlab function using equations

$$I_{dm\omega_{max}} = I_{m\omega_{max}} \sin(\gamma_{\omega_{max}}) \tag{17}$$

$$I_{qm\omega_{max}} = I_{m\omega_{max}} \cos(\gamma_{\omega_{max}}) \tag{18}$$

$$\Psi_{d\omega_{max}} = \Psi_{md} + L_d I_{dm\omega_{max}} + L_{dq} I_{qm\omega_{max}} \tag{19}$$

$$\Psi_{q\omega_{max}} = \Psi_{mq} + L_q I_{qm\omega_{max}} + L_{dq} I_{dm\omega_{max}} \tag{20}$$

$$\Psi_{s\omega_{max}} = \Psi_{d\omega_{max}} + \mathrm{j}\Psi_{q\omega_{max}} \tag{21}$$

$$V_{\omega_{max}} = \mathrm{j}\omega_{max}\Psi_{s\omega_{max}} + \tag{22}$$

$$(R_s + \mathrm{j}L_{ew}\omega_{max}) I_{m\omega_{max}} e^{\mathrm{j}(\frac{\pi}{2} + |\gamma_{\omega_{max}}|)} \tag{23}$$

$$ceq = |V_r| - |V_{\omega_{max}}| \tag{24}$$

where L_{ew} is the analytically calculated end winding leakage inductance (normally not directly extracted from 2D FE simulations), and V_r is the complex voltage vector at motor terminals calculated using the same equations, but with rated current magnitude I_{mr} and rated current control angle γ_r. The voltage V_r is calculated outside constrained nonlinear optimization and is used as an input parameter. This internal optimization within the global optimization performed using DE algorithm consumes very little time since it uses constant motor parameters and algebraic equations.

The values of $\gamma_{\omega_{max}}$ and $I_{m\omega_{max}}$ calculated in step 1 are not quite correct since they use motor parameters extracted from FE simulation at rated speed, current and control angle. Therefore, in this step a new magnetostatic 2D FE simulation must be performed with current vector defined by $\gamma_{\omega_{max}}$ and $I_{m\omega_{max}}$ from step 1. From this simulation, after freezing the permeabilities, new values of PM flux and inductances are extracted. The CNO is used again to calculate new values of $\gamma_{\omega_{max}}$ and $I_{m\omega_{max}}$ which are compared to the values from the previous step. If their difference is smaller than some initially prescribed margin, e.g. 0.1 %, the last calculated $\gamma_{\omega_{max}}$ and $I_{m\omega_{max}}$ are the results used for calculation of $P_{em\omega_{max}}$. If the difference is greater than the margin, step 2 is repeated always using $\gamma_{\omega_{max}}$ and $I_{m\omega_{max}}$ from the previous iteration in magnetostatic FE simulation to calculate new values of PM flux and inductances until the difference between current control angle and current

vector magnitude at maximum speed from two consecutive iterations is smaller than the margin.

3 From the last FE simulation core losses should be calculated and together with mechanical losses used to calculate the output shaft power

$$P_{out\omega_{max}} = P_{em\omega_{max}} - P_{c\omega_{max}} - P_{mech,w\omega_{max}} \quad (25)$$

4 Thus calculated $P_{out\omega_{max}}$ is used to evaluate the inequality constraint which requires that $P_{out\omega_{max}} \geq P_{out\omega_r}$.

Optimization results: The result of the optimization procedure is a lamination cross-section of a reference design, shown in Fig. 7a (welding channels are added on outer stator and rotor side). With a prescribed stack length of 312 mm and slot current density of 6 A/mm^2, this motor has output power of 106 kW, which is more than the required output power of the largest motor in the series. To match the output power of 100 kW, stack length or current density can be reduced. It is better to use the maximum stack length for the prototype motor and leave some current density margin (thermal margin) for the testing phase.

The power ratings of the motors in the series have a ratio 2:3:4 so this will also be the ratio of the stack lengths for the 50 kW, 75 kW and 100 kW motors respectively. In order to use technologically convenient magnet plates, rotors of the machines will be made of 4, 6 and 8 segments, where each segment has one magnet plate in axial direction (Fig. 7b). Output power and shaft torque behaviour of the machines with target power of 50 kW, 75 kW and 100 kW is shown in Fig. 4, where one can see that all machines satisfy CPSR of more than 1.5x since it was not bounded from the upper side during optimization.

Details on winding, segments, magnet plates and flux weakening (FW) behaviour for the motors in the series are given in Tab. 1. Two most important parameters that define power vs speed output, saliency ratio and characteristic current, are essentially equal in all three cases. This is expected behaviour due to the nature of analytical axial scaling laws ([14, 15]) and it is the reason why output power vs. speed curves in Fig. 4 have identical behaviour.

Table 1: Details on winding, segments, magnet plates and FW behaviour

Target power rating, kW	**100**	**75**	**50**
Rated speed, rpm		**3000**	
Number of parallel circuits		1	
Number of turns per coil	2	3	4
Number of rotor/magnet segments	8	6	4
Magnet plate length, mm		39	
Total number of magnet plates	320	240	160
Saliency ratio	2,14	2,13	2,11
Characteristic current, pu	1,37	1,36	1,34

Table 2 provides data on power and torque densities (per mass and per volume) for the 100 kW prototype. A distinction between active machine mass and volume and total machine mass and volume has been made since in our case the manufacturer of the prototype used heavy steel housing. For example, in the case of aluminium housing, the power/total weight ratio will be definitely greater than for the case of iron housing even if the motor has the same ratio of power/active weight (laminations, magnets and copper). It is confirmed that power density of this PMSynRM motor is significantly higher (0.40 kW/kg) than that for an equivalent size squirrel-cage induction motor (SCIM) according to the literature ([1], 0.10-0.11 kW/kg) or to our manufacturer's experience (30 kW, 220 kg = 0.14 kW/kg).

Table 2: Power and torque densities of 100 kW prototype

Power / total mass	100 kW / 252 kg	0.40 kW / kg
Power / active mass	100 kW / 138 kg	0.72 kW / kg
Power / total volume	100 kW / 33.15 L	3.02 kW / L
Torque / total mass	318 Nm / 252 kg	1.26 Nm / kg
Torque / active mass	318 Nm / 138 kg	2.30 Nm / kg
Torque / total volume	318 Nm / 33.15 L	9.59 Nm / L

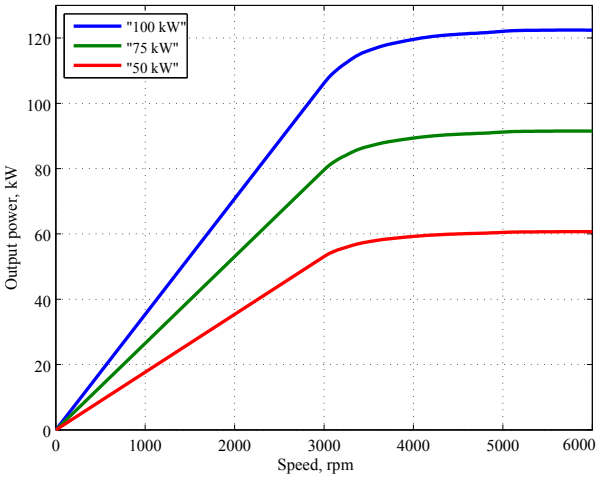

Fig. 4: Output power vs. speed for machines of target power 50 kW, 75 kW and 100 kW

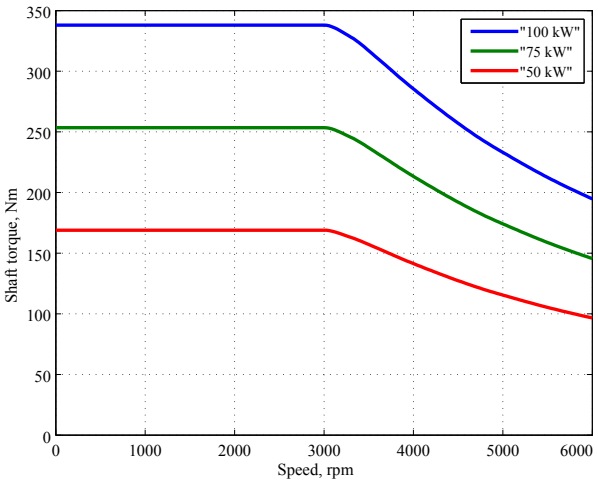

Fig. 5: Shaft torque vs. speed for machines of target power 50 kW, 75 kW and 100 kW

Thermal analysis: By using pre-optimization study considering technology, housing size and cooling properties, a thermal limit of maximum allowed total loss of 4590 W to be used as an optimization boundary constraint was determined. The copper and magnet temperatures for rated load operating point were estimated to be 140 °C and 130 °C respectively. These values were used as constant value variables inside optimization procedure to determine temperature dependent copper resistivity and permanent magnet remanent flux density.

Post-optimization thermal calculation was conducted in Motor-CAD software using iterative calculation approach. Initially calculated losses (electromagnetic and mechanical) are used as an input to thermal lumped network calculation which gives temperatures as outputs. These temperatures are then used to correct the temperature dependent electromagnetic losses. By repeating this procedure, final stationary temperatures are obtained. Calculated active winding average temperature was 139 °C, which is almost identical with the initial assumption of 140 °C. Permanent magnet temperature could not be exactly determined since rotor geometry we used did not exist in this template-based software at the time.

Mechanical stress analysis: Due to the complicated geometry of the PMSynRM machine and existence of permanent magnets, a special care must be taken to calculate the maximum stress in the rotor. A pre-optimization mechanical stress study was used to determine air gap, outer layer and inner layer rotor bridge thicknesses to be used as constant value variables during optimization.

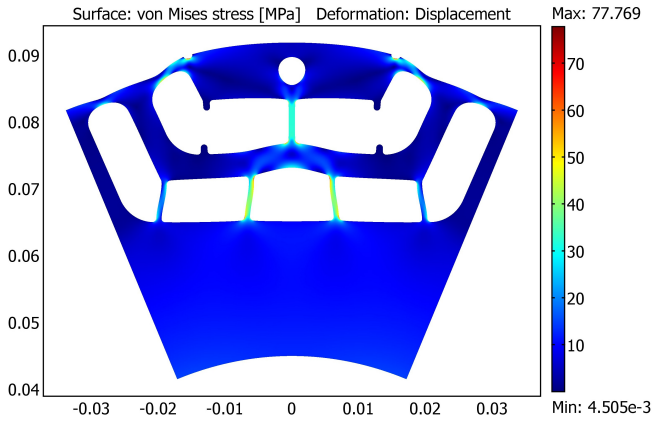

Fig. 6: Mechanical stress at 4500 rpm

The post-optimization stress analysis was preformed using 2D FE calculation in COMSOL Multiphysics at the speed 50 % above rated speed (4500 rpm). In order to take into account the centrifugal force on the iron part of the rotor, the load components were set parametrically using the relation

$$F_x = \rho_{Fe}\omega_m^2 x$$
$$F_y = \rho_{Fe}\omega_m^2 y \tag{26}$$

where ρ_{Fe} is the density of the rotor material and ω_m is the rotational speed of the rotor. Symmetry boundaries are used along the edges where rotor was cut to model the remainder of the rotor.

An additional stress to the rotor iron caused by the centrifugal force on the magnets is taken into account as the pressure to the outer radial contact between magnet and rotor cavity. The pressure can be expressed as

$$F_y = \rho_{PM}\omega_m^2 \cdot R_i \tag{27}$$

where ρ_{PM} is the density of the permanent magnet material and R_i is the distance between center of rotation and the i^{th} magnet.

As it is shown in (26) and (27), the load forces depend only on square of the rotational speed, assuming there is no significant deformation in the displacement (x and y). The rotor material was modelled using Young's modulus ($E = 200$ GPa) and Poisson's ratio ($\nu = 0.3$). The maximal stress of 77.8 MPa occurred at one of the bridges, shown in Fig. 6. Yield strength of 282 MPa was used to calculate safety factor k_s=3.6. Due to the usage of the linear isotropic material in the solver and the assumption of small deformation, it is possible to recalculate maximal stress for the centrifugal loading at any speed

$$S_{new} = \left(\frac{\omega_{new}}{\omega_{calc}}\right)^2 S_{calc} \tag{28}$$

Using (28) it is possible to calculate maximum speed of the rotor for the defined safety factor (k_s).

$$\omega_{max} = \omega_{calc}\sqrt{\frac{S_{max}}{k_s \cdot S_{calc}}} \tag{29}$$

In this case, the theoretically highest speed for safety factor k_s = 1 is 8567 rpm.

Measurements: A 100 kW machine (IEC 180 frame size, forced air cooling) was built as a test prototype. A detail from manufacturing of rotor segment before insertion of magnets is shown in Fig. 7b. The prototype was tested in the laboratory equipped with 450 kW IPM load machine (Fig. 8) and ABB ACS800 Multidrive system. The details on precision of measurement equipment are given in Tab. 3. In other words, the inverters for both the tested machine and the load machine are sharing the DC link which allows the energy between the motor (tested machine) and the generator (load machine) to circulate while the losses are supplied from the mains. Along with the measurement of electrical quantities, temperature, torque and speed, special measurement subsystem was created for estimation of current control angle. Since inverters use direct torque control (DTC), the exact position of current vector is not known, therefore current waveform and rotor position from encoder were used in order to decompose current vector into components to confirm the calculated MTPA parameters. It was not possible to extract the exact value of magnet losses and mechanical windage and friction losses (the machine is cooled by an external fan) during load test. It was considered that these values are accurately calculated in the design stage. Therefore, the iron losses were determined as a difference between total measured losses, copper losses and estimated sum of magnet losses and friction and windage losses.

The comparison of measured and calculated results is shown in Table 4. The difference in measured and calculated copper losses occurs primarily due to the difference in measured and calculated current needed to produce the required shaft torque. The winding is made of Litz wire so proximity and eddy current losses are neglected although if the PWM shaped current waveform can be predicted in the design stage, those additional losses can be accounted for, without the loss of generality of the presented approach.

The difference in measured and calculated iron losses is less than 10 %, which can be considered a good match taking into account the key uncertainties in iron loss calculation. The first uncertainty comes from the power loss curves of steel lamination manufacturer which are normally not available for higher frequencies (5th or 7th harmonic with respect to rated fundamental frequency of 200 Hz in this case). The second uncertainty comes from the loss increase due to motor lamination manufacturing process: laser cutting or stamping. These processes severely deteriorate electromagnetic properties of the electrical steel in the vicinity of stator slots and rotor cavities. The third uncertainty comes from PWM control and its effect on the current waveform shape and added harmonics in the magnetic field. These three influences are taken into the account by using a correcting factor of 1.5 (experience based) which multiplies core losses calculated using FE model. It is easy to conclude that if this factor were only 6.8 % larger (i.e. equal to 1.602), which is still realistic considering the current waveform shape of the inverter used, we would have obtained a perfect match in the calculation of core losses. Efficiency vs. speed curve at constant rated load 318 Nm is shown in Fig. 9, while power factor vs. speed is shown in Fig. 10.

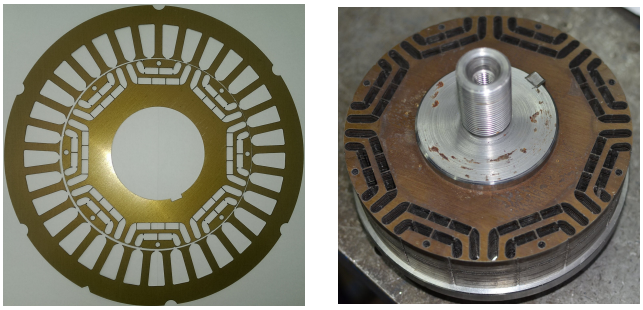

(a) Lamination cross section (b) Rotor segment without magnets

Fig. 7: Manufactured prototype

Fig. 8: 100 kW prototype and 450 kW load machine

Table 3: Test-bench details

Sensor	Type	Accuracy
Torque	HBM T40, 3000 Nm	0,05 %
Current	ABB ES500-9647, 500 A	0,5 %
Voltage	built-in LEM NORMA 4000	0,1 %
Speed	encoder WACHENDORFF WDG 58B	0,01 %

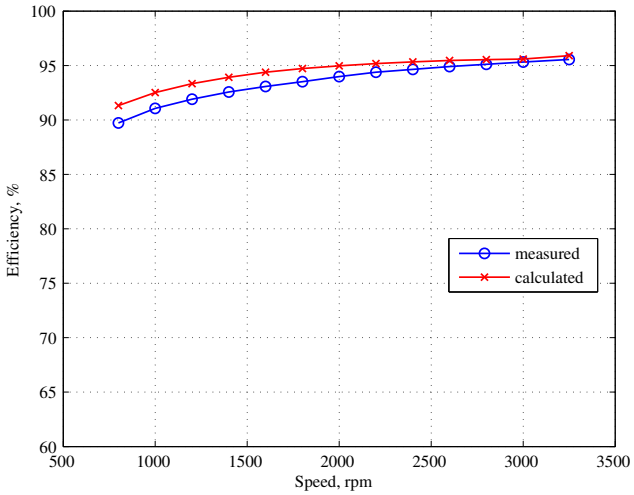

Fig. 9: Efficiency vs. speed curve at constant rated load 318 Nm

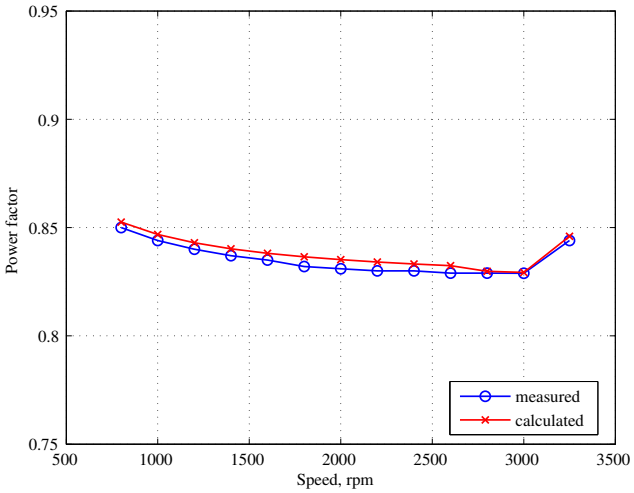

Fig. 10: Power factor vs. speed curve at constant rated load 318 Nm

Table 4: Comparison of calculated and measured results at 100 kW, 3000 rpm

	Calculation	Measurement	Difference
T, Nm	317,9	318,3	0,1 %
I_1, A	204,9	212,6	3,8 %
I, A	207,1	215,0	3,8 %
γ, °	-44,8	-39,9	-10,9 %
P_{out}, kW	99,9	100,0	0,1 %
P_{el}, kW	104,5	104,9	0,4 %
η, %	95,60	95,32	-0,3 %
P_{loss}, W	4597	4911	6,8 %
P_{Cu}, W	2016	2172	7,8 %
P_{Fe}, W	2522	2679	6,2 %
P_{mag}, W	35,7		
P_{mech}, W	23,5		

Conclusion: This paper presents a reliable and effective methodology for optimizing a series of PMSynRMs using combined analytical-FE model of the motor. It combines some of the best practices for definition and execution of optimization problems found in literature with some original contributions presented in detail in the paper. Those already established practices include definition of optimization variables as non-dimensional ratios, normalization of inequality constraints and their handling without using penalty functions embedded into cost function, and optimization without variation of the number of turns per coil and/or the number of parallel paths.

The first contribution introduced in the paper is a time effective and accurate method for calculation of peak transient stator winding short-circuit current to determine the level of demagnetization of permanent magnets during sudden three-phase short circuit at the motor terminals using only magnetostatic FE calculations. This calculation is useful for designing fault tolerant motors. The second contribution is an accurate method for calculation of maximum power output at maximum speed using magnetostatic FE simulation considering the voltage and current limits of the power supply and motor. The method is suitable for PMSynRMs with either finite or infinite theoretical maximum speed limit and is very useful for verifying whether or not the motor's CPSR meets the design specifications. Both methods are computationally efficient so they can be used for every population member of a stochastic optimization algorithm, like Differential Evolution used in this paper.

The optimization approach presented in the paper was used to design a PMSynRM rated 100 kW with excellent torque per volume capabilities, fitted into an IEC180 frame size housing previously used for an existing 2 pole, 30 kW IE1 induction motor. A prototype was built and tested in order to verify the calculation results by comparing them to measurements.

Acknowledgment: The research and prototype manufacturing has been supported by electric machine manufacturing companies Končar-MES d.o.o. and TEMA d.o.o.

References

1 A. de Almeida, F. Ferreira, and A. Quintino Duarte, "Technical and economical considerations on super high-efficiency three-phase motors," *Industry Applications, IEEE Transactions on*, vol. 50, no. 2, pp. 1274–1285, March 2014.

2 A. de Almeida, F. Ferreira, and G. Baoming, "Beyond induction motors;technology trends to move up efficiency," *Industry Applications, IEEE Transactions on*, vol. 50, no. 3, pp. 2103–2114, May 2014.

3 M. Barcaro, N. Bianchi, and F. Magnussen, "Permanent-magnet optimization in permanent-magnet-assisted synchronous reluctance motor for a wide constant-power speed range," *IEEE Transactions on Industrial Electronics*, vol. 59, no. 6, pp. 2495–2502, June 2012.

4 J. Haataja and J. Pyrhönen, "Permanent magnet assisted synchronous reluctance motor: an alternative motor in variable speed drives," in *Energy Efficiency in Motor Driven Systems*, F. Parasiliti and P. Bertoldi, Eds. Springer Berlin Heidelberg, 2003, pp. 101–110.

5 I. Boldea, L. Tutelea, and C. Pitic, "Pm-assisted reluctance synchronous motor/generator (pm-rsm) for mild hybrid vehicles: electromagnetic design," *IEEE Transactions on Industry Applications*, vol. 40, no. 2, pp. 492–498, March 2004.

6 P. Niazi, H. Toliyat, D.-H. Cheong, and J.-C. Kim, "A low-cost and efficient permanent-magnet-assisted synchronous reluctance motor drive," *IEEE Transactions on Industry Applications*, vol. 43, no. 2, pp. 542–550, March 2007.

7 T. Tokuda, M. Sanada, and S. Morimoto, "Influence of rotor structure on performance of permanent magnet assisted synchronous reluctance motor," in *International Conference on Electrical Machines and Systems, ICEMS*, Nov 2009, pp. 1–6.

8 K. Khan, M. Leksell, and O. Wallmark, "Design aspects on magnet placement in permanent-magnet assisted synchronous reluctance machines," in *5th IET International Conference on Power Electronics, Machines and Drives (PEMD)*, April 2010, pp. 1–5.

9 A. Vagati, B. Boazzo, P. Guglielmi, and G. Pellegrino, "Ferrite assisted synchronous reluctance machines: A general approach," in *International Conference on Electrical Machines (ICEM)*, Sept 2012, pp. 1315–1321.

10 R. Vartanian, Y. Deshpande, and H. Toliyat, "Performance analysis of a rare earth magnet based nema frame permanent magnet assisted synchronous reluctance machine with different magnet type and quantity," in *IEEE International Electric Machines Drives Conference (IEMDC)*, May 2013, pp. 476–483.

11 H. de Kock and M. Kamper, "Dynamic control of the permanent magnet-assisted reluctance synchronous machine," *IET Electric Power Applications*, vol. 1, no. 2, pp. 153–160, March 2007.

12 S. Rick, M. Felden, M. Hombitzer, and K. Hameyer, "Permanent magnet synchronous reluctance machine - bridge design for two-layer applications," in *IEEE International Electric Machines Drives Conference (IEMDC)*, May 2013, pp. 1376–1383.

13 S. Rick, A. Putri, D. Franck, and K. Hameyer, "Permanent magnet synchronous reluctance machine; design guidelines to improve the acoustic behavior," in *International Conference on Electrical Machines (ICEM*, Sept 2014, pp. 1383–1389.

14 D. Zarko and S. Stipetic, "Criteria For Optimal Design Of Interior Permanent Magnet Motor Series," in *XXth International Conference On Electrical Machines (ICEM), 2012*, Sept 2012, pp. 1242–1249.

15 S. Stipetic, D. Zarko, and M. Popescu, "Scaling Laws for Synchronous Permanent Magnet Machines," in *Tenth International Conference on Ecological Vehicles and Renewable Energies (EVER), 2015*, April 2015, pp. 1–7.

16 R. Storn and K. Price, "Differential Evolution - a Simple and Efficient Adaptive Scheme for Global Optimization over Continuous Spaces," *Technical Report TR-95-012, ICSI*, March 1995.

17 D. Zarko, D. Ban, and T. Lipo, "Design Optimization of Interior Permanent Magnet (IPM) Motors with Maximized Torque Output in the Entire Speed Range," in *European Conference on Power Electronics and Applications*, 2005, pp. 10 pp.–P.10.

18 W. Ouyang, D. Zarko, and T. Lipo, "Permanent Magnet Machine Design Practice and Optimization," in *Conference Record of the 2006 IEEE Industry Applications Conference*, vol. 4, Oct 2006, pp. 1905–1911.

19 G. Sizov, D. Ionel, and N. Demerdash, "Multi-objective optimization of PM AC machines using computationally efficient - FEA and differential evolution," in *IEEE International Electric Machines Drives Conference (IEMDC)*, May 2011, pp. 1528–1533.

20 Y. Duan and D. Ionel, "A Review of Recent Developments in Electrical Machine Design Optimization Methods With a Permanent-Magnet Synchronous Motor Benchmark Study," *IEEE Transactions on Industry Applications*, vol. 49, no. 3, pp. 1268–1275, May 2013.

21 P. Zhang, D. Ionel, and N. Demerdash, "Saliency Ratio and Power Factor of IPM Motors Optimally Designed for High Efficiency and Low Cost Objectives," in *IEEE Energy Conversion Congress and Exposition (ECCE)*, Sept 2014, pp. 3541–3547.

22 P. Zhang, G. Sizov, D. Ionel, and N. Demerdash, "Establishing the Relative Merits of Interior and Spoke-Type Permanent Magnet Machines with Ferrite or NdFeB Through Systematic Design Optimization," *IEEE Transactions on Industry Applications*, vol. PP, no. 99, pp. 1–1, 2015.

23 Y. Duan and D. Ionel, "Nonlinear Scaling Rules for Brushless PM Synchronous Machines Based on Optimal Design Studies for a Wide Range of Power Ratings," *IEEE Transactions on Industry Applications*, vol. 50, no. 2, pp. 1044–1052, March 2014.

24 X. Liu and G. Slemon, "An Improved Method of Optimization for Electrical Machines," *IEEE Transactions on Energy Conversion*, vol. 6, no. 3, pp. 492–496, Sep 1991.

25 J. Lampinen, "Multi-Constrained Nonlinear Optimization By The Differential Evolution Algorithm," in *6th On-Line World Conference On Soft Computing In Industrial Applications (Wsc6)*, 2001, pp. 1–19.

26 K.-C. Kim, J. Lee, H. J. Kim, and D.-H. Koo, "Multiobjective Optimal Design for Interior Permanent Magnet Synchronous Motor," *IEEE Transactions on Magnetics*, vol. 45, no. 3, pp. 1780–1783, March 2009.

27 M. Martinovic, D. Zarko, S. Stipetic, T. Jercic, M. Kovacic, Z. Hanic, and D. Staton, "Influence of winding design on thermal dynamics of permanent magnet traction motor," in *International Symposium on Power Electronics, Electrical Drives, Automation and Motion (SPEEDAM), 2014*, June 2014, pp. 397–402.

28 P. Zhang, G. Sizov, M. Li, D. Ionel, N. Demerdash, S. Stretz, and A. Yeadon, "Multi-Objective Tradeoffs in the Design Optimization of a Brushless Permanent-Magnet Machine With Fractional-Slot Concentrated Windings," *IEEE Transactions on Industry Applications*, vol. 50, no. 5, pp. 3285–3294, Sept 2014.

29 G. Pellegrino and F. Cupertino, "FEA-based Multi-Objective Optimization of IPM Motor Design Including Rotor Losses," in *IEEE Energy Conversion Congress and Exposition (ECCE)*, Sept 2010, pp. 3659–3666.

30 N. Bianchi, D. Durello, and E. Fornasiero, "Multi-Objective Optimization of a PM Assisted Synchronous Reluctance Machine, Including Torque and Sensorless Detection Capability," in *6th IET International Conference on Power Electronics, Machines and Drives (PEMD 2012)*, March 2012, pp. 1–6.

31 M. Meyer and J. Bocker, "Transient peak currents in permanent magnet synchronous motors for symmetrical short circuits," in *International Symposium on Power Electronics, Electrical Drives, Automation and Motion, SPEEDAM*, May 2006, pp. 404–409.

32 D. Zarko, D. Ban, and R. Klaric, "Finite Element Approach to Calculation of Parameters of an Interior Permanent Magnet Motor," *Automatika*, vol. 46, no. 3–4, pp. 113–122, 2005.

33 W. L. Soong and T. J. E. Miller, "Field-weakening performance of brushless synchronous ac motor drives," *IEE Proceedings - Electric Power Applications*, vol. 141, no. 6, pp. 331–340, Nov 1994.

34 R. Schiferl and T. Lipo, "Power Capability Of Salient Pole Permanent Magnet Synchronous Motors In Variable Speed Drive Applications," *IEEE Transactions On Industry Applications*, vol. 26, no. 1, pp. 115–123, 1990.